

1 Deep autoregressive generative models capture the 2 intrinsics embedded in T-cell receptor repertoires

3 Yuepeng Jiang¹ and Shuai Cheng Li^{1*}

4 ¹Department of Computer Science, City University of Hong Kong, Kowloon Tong, Hong Kong

5 *shuaicli@cityu.edu.hk

6 ABSTRACT

T-cell receptors (TCRs) play an essential role in the adaptive immune system. Probabilistic models for TCR repertoires can help decipher the underlying complex sequence patterns and provide novel insights into understanding the adaptive immune system. In this work, we develop TCRpeg, a deep autoregressive generative model to unravel the sequence patterns of TCR repertoires. TCRpeg outperforms state-of-the-art methods in estimating the probability distribution of a TCR repertoire, boosting the accuracy from 0.672 to 0.906 measured by the Pearson correlation coefficient. Furthermore, with promising performance in probability inference, TCRpeg improves on a range of TCR-related tasks: revealing TCR repertoire-level discrepancies, classifying antigen-specific TCRs, validating previously discovered TCR motifs, generating novel TCRs, and augmenting TCR data. Our results and analysis highlight the flexibility and capacity of TCRpeg to extract TCR sequence information, providing a novel approach to decipher complex immunogenomic repertoires.

keywords: T-cell receptor repertoires, deep neural networks, probabilistic inference, immunoinformatics

8 Introduction

9 The adaptive immune system consists of highly diverse B and T-cells whose unique receptors can recognize
10 enormous pathogens in vertebrates. The generation of these highly diverse receptors arises mainly from
11 the genetic recombination of DNA segments from V, D, and J genes through V(D)J recombinations^{1,2}.
12 T-cells play an essential role in antiviral defense by selectively eliminating virus-infected cells³. Their
13 ability to recognize specific short peptides; that is, peptide antigens bound to the major histocompatibility

1 complex (MHC) molecules are determined primarily by their unique receptor proteins^{4,5}. A receptor
2 contains an α polypeptide chain and an β polypeptide chain, both of which consist of two extracellular
3 domains: the variable (V) region and the constant (C) region⁶. The variable regions of the TCR α - and β -
4 chains both have three complementarity-determining regions (CDRs) that contribute to the specificity of
5 antigen recognition. Among these CDRs, the CDR3 region of the TCR β chain plays a pivotal role in the
6 recognition of the peptides presented by MHC. In contrast, the CDR1 and CDR2 regions contribute minor
7 effects to direct antigen recognition^{6,7}. Due to the importance of the highly diverse CDR3 region of the
8 TCR β chain in antigen recognition and data availability, this work focuses on deciphering the underlying
9 pattern of the CDR3 sequence.

10 Advancement in high-throughput sequencing techniques of the T-cell receptor repertoire provides a
11 census of T-cells found in blood or tissue samples⁸⁻¹¹. Large-scale sequencing data promote the investiga-
12 tion of the composition of immune repertoires, characterizing adaptive immune responses, and developing
13 descriptive models. The sampled repertoire of TCR serves as an indicator of the complete repertoire, re-
14 flecting the pathogenic history or the immune response to stimuli¹²⁻¹⁵, with clinical applications including
15 cancer prediction and anticipation of immunotherapy. For example, Han *et al.* developed a statistical
16 index named TIR index based on TCR to predict response and survival outcomes after immunotherapy¹⁶.
17 Beshnova *et al.* defined a cancer score for a given patient based on the predictive model trained on specific
18 TCR sequences that are assumed to be simply associated with cancers¹⁷.

19 Despite the success in predictive tasks associated with T-cell repertoires, precise probabilistic dis-
20 tribution modeling is demanding. Given that TCR repertoires possess extremely large diversity, the
21 sampled repertoires from different samples, or even from the same donors will often differ significantly.
22 Consequently, characterizing the sequence pattern of a given repertoire from a probabilistic manner is
23 more reliable than modeling with raw TCR sequences and read counts, with many potential applications
24 such as estimating the relative ratio of CD4⁺ to CD8⁺^{18,19} and investigating the differences in sequence
25 characteristics between functional T-cell subsets^{20,21}. Conventionally, modeling the sequence pattern
26 behind a TCR repertoire is disentangled into two processes: generation (V(D)J recombination)^{22,23} and
27 selection^{19,24,25}. The ultimate probability assigned to a TCR sequence is the product of the selection factor
28 and the generation probability inferred from the selection process and the generation process, respectively.

1 However, the generation models learned from different individuals share a high mutual similarity^{22,25},
2 indicating that the selection process plays a central role in discriminating the TCR repertoires sampled
3 from different individuals. Therefore, instead of two-step disentanglement, we can infer the probability of
4 TCR sequences end-to-end.

5 In this work, we introduce a new probabilistic model, TCRpeg, that utilizes deep learning techniques to
6 learn the underlying sequence patterns of TCR repertoires. Specifically, TCRpeg employs the architecture
7 of the deep autoregressive model with gated recurring units (GRU)²⁶ layers to characterize the repertoire
8 through the flexible and non-linear structure of deep neural networks. TCRpeg can infer the sequence
9 probability distribution with higher accuracy than other probabilistic models, boosting the performance
10 from 0.672 to 0.906 measured by the Pearson correlation coefficient. We then applied the model to profile
11 TCR subrepertoires and found that a simple probabilistic classifier can achieve high predictive performance.
12 TCRpeg also provides high-quality latent vector representations for TCR sequences. Based on these vector
13 encodings of TCR sequences, we built a fully connected neural network to classify the cancer-associated
14 TCRs and SARS-CoV-2 epitope-specific TCRs, achieving 0.844 and 0.872 AUC, respectively; higher than
15 DeepCAT¹⁷'s AUC 0.768 but slightly lower than TCRGP²⁷'s AUC 0.882. As a generative model, TCRpeg
16 can generate new TCR sequences, among which more than 50% share the same antigen specificity as the
17 sequences used in training according to the TCRMATCH²⁸ with a scoring threshold of 0.90, while the other
18 two generative models, TCRvae²⁹ and soNNia¹⁹, achieve a proportion of less than 40%. Further, TCRpeg
19 helps data augmentation; it shows a 7.4% accuracy gain in predicting cancer-associated TCRs using the
20 DeepCAT¹⁷ model.

21 **Results**

22 **Autoregressive generative model for TCR sequences**

23 Previously, the probabilistic sequence pattern of a TCR repertoire was modeled by the two disentangled
24 processes of generation^{22,23} and selection^{19,24,25} (e.g., soNNia¹⁹) or the variational autoencoder with
25 convolutional neural networks (CNNs) as encoder and decoder (TCRvae²⁹). Although both models
26 achieved satisfactory performance, they lack the elegance to handle variable-length TCR sequence data.
27 The two types of models pad each sequence to a fixed length with an extra token representing the padding

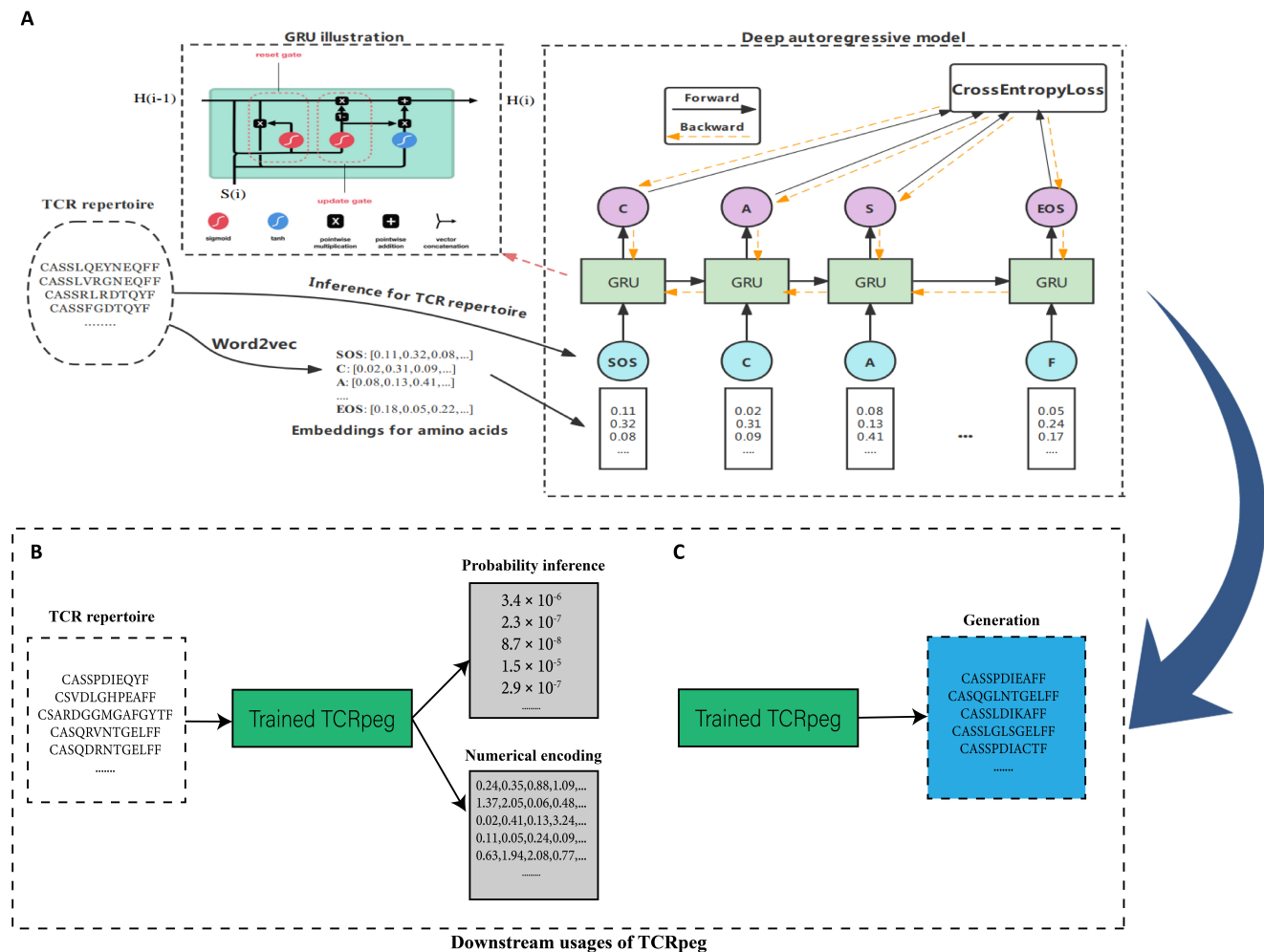


Figure 1. Workflow of TCRpeg to infer probabilistic patterns of immune receptor repertoires. (A) We have implemented a deep autoregressive network with GRU layers to process TCR sequences of different lengths to learn the hidden sequence pattern. The word2vec algorithm is first applied to the TCR repertoire to learn the numerical representations of each amino acid, regarding amino acids and TCR sequences as “Words” and “Sentences”. Then the TCR sequence is inputted into the deep autoregressive model sequentially. The model is updated by the gradient descent algorithm with the cross-entropy loss between the output logits and true labels. The trained TCRpeg model can be readily extended to downstream usages, including probability inference, encoding TCRs (B), and generating similar new TCRs (C). These functions and applications of TCRpeg are further elaborated in the Results section.

1 positions. However, the introduction of the extra token could introduce noise to the original data and
 2 partially conceal useful information about the diversity of sequence lengths, which is important for antigen
 3 specificity^{30,31}.

4 In the past decade, deep learning models have achieved considerable success in handling sequential
 5 data^{26,32–35}. An autoregressive model processes the sequential data using observations from previous
 6 stages to infer the entry at the next time point. In the context of the TCR sequence, we can apply an
 7 autoregressive model to infer a residue using the amino acid subsequence proceeding from it. Therefore,
 8 we built TCRpeg, an autoregressive model that formulates the probability of a TCR sequence \mathbf{x} as $p(\mathbf{x}|\theta)$,

1 where the parameters θ capture the latent evolutionary patterns to generate \mathbf{x} . The probability density
2 $p(\mathbf{x}|\theta)$ can be calculated by the product of probabilities conditioned on previous residues along a sequence
3 with length L through an autoregressive likelihood

$$p(\mathbf{x}|\theta) = p(x_1|\theta) \prod_{i=2}^L p(x_i|x_1, \dots, x_{i-1}; \theta). \quad (1)$$

4 Figure 1 shows the TCRpeg workflow. We utilized gated recurrent units (GRUs)²⁶, commonly adopted in
5 recurrent neural networks, to model the autoregressive likelihood (Methods). Recurrent neural network
6 models might encounter a gradient explosion for long peptide sequences^{36,37}. However, TCR sequences
7 contain mainly 12 to 17 residues (Supplementary S1). Thus, we can parameterize the generative process
8 with feed-forward GRU models that aggregate dependencies in sequences through the transmitting hidden
9 features controlled by the gate functions.

10 Training a GRU model requires vector representations for each amino acid. Instead of using one-hot
11 encodings or predefined characteristics of the analysis of principal components in biochemical features¹⁷,
12 we adopted the word2vec algorithm³⁸ to adaptively learn the embeddings for each amino acid from the TCR
13 sequencing data by treating an amino acid as a “Word” and each TCR sequence as a “Sentence” (Method).
14 Then, TCRpeg can be trained in a forward language modeling manner. To estimate the probability of a
15 given TCR sequence, we applied Eq.1 to the pre-trained TCRpeg. Details of the architecture of TCRpeg,
16 the training, and inferring processes are included in the Methods.

17 **TCRpeg infers functional TCR repertoire probability distribution**

18 First, we evaluated the probability distribution of the TCR sequences inferred by TCRpeg and compared
19 its accuracy with the other two probabilistic models, soNNia¹⁹ and TCRvae²⁹. To assess and compare
20 their performance, we constructed a universal TCR repertoire from a large cohort of 743 individuals from
21 Emerson *et al.*³⁹, following a similar data preprocessing strategy in Isacchini *et al.*¹⁹. Specifically, we
22 pooled the unique nucleotide sequences of TCRs from all individuals and constructed a universal TCR
23 repertoire. The universal repertoire was randomly divided into training and testing subrepertoires by a
24 50:50 split to ensure consistency with soNNia¹⁹ and TCRvae²⁹. Then we trained TCRpeg, soNNia, and
25 TCRvae on the training set (Methods).

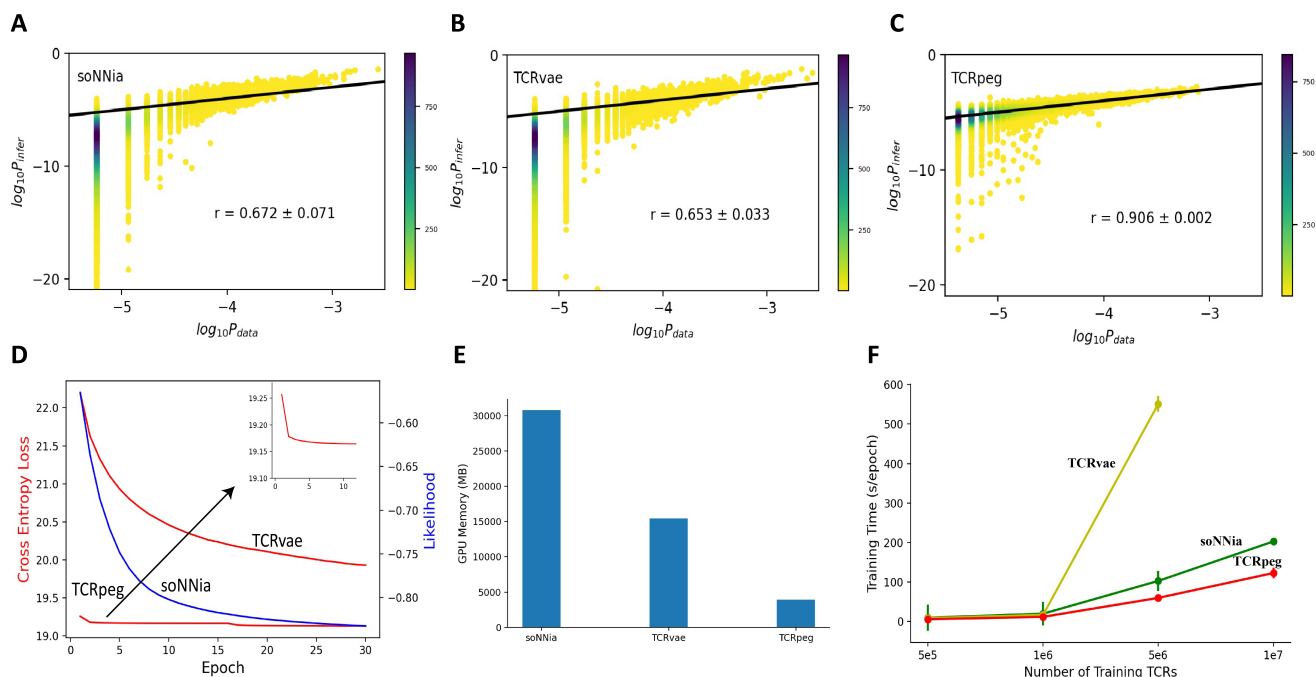


Figure 2. Performance of TCRpeg compared to the other two baseline methods soNNia and TCRvae. (A-C) Scatterplots of observed frequency P_{data} vs. estimated probability P_{infer} for (A) soNNia, (B) TCRvae and (C) TCRpeg models trained on the large TCR pool combining 743 individuals from Emerson *et al.*³⁹, along with the corresponding Pearson correlation coefficient r . The color indicates the number of sequences. (D-F) Comparison of soNNia, TCRvae, and TCRpeg model from practical aspects. Experiments are conducted under the same settings (learning rate and batch size) on a single Nvidia Tesla V100 GPU card with maximum 32 gigabytes memory. (D) The training curves for these three models. The soNNia model uses the model objective function (shown in the blue curve), while TCRvae and TCRpeg model minimize the cross-entropy loss (shown in the red curves). TCRpeg only needs less than ten epochs to converge, while the other two take around 30 epochs to converge. (E) The bar plot shows the GPU memory required to train each model. TCRpeg is more hardware-friendly. (F) The training speed of each model. TCRpeg takes less time to complete one training epoch compared to soNNia and TCRvae.

1 We evaluated the three models, each to estimate a probability distribution $P_{infer}(\mathbf{x})$ for the test set;
 2 TCRpeg shows high accuracy with substantial improvement over soNNia and TCRvae, but requires
 3 lower resources to train. Prediction accuracy can be quantified using the Pearson correlation coefficient r
 4 between the inferred and true probability distributions, i.e., $P_{infer}(\mathbf{x})$ and $P_{data}(\mathbf{x})$, on the test set (Methods).
 5 TCRpeg achieved $r \simeq 0.906$; however, soNNia and TCRvae obtained $r \simeq 0.672$ and $r \simeq 0.653$, respectively
 6 (Fig. 2A-2C). TCRpeg also performs stably and robustly when training on a small proportion of training
 7 data consisting of only 2×10^5 TCR sequences (Supplementary S2). In addition to the substantial
 8 accuracy improvement, TCRpeg converges faster and costs significantly less GPU memory (Fig. 2D-2F).
 9 It converges within five epochs, whereas the other two methods require around 30 epochs. Moreover,
 10 SoNNia and TCRvae consume six times and three times more memory than TRCpeg.

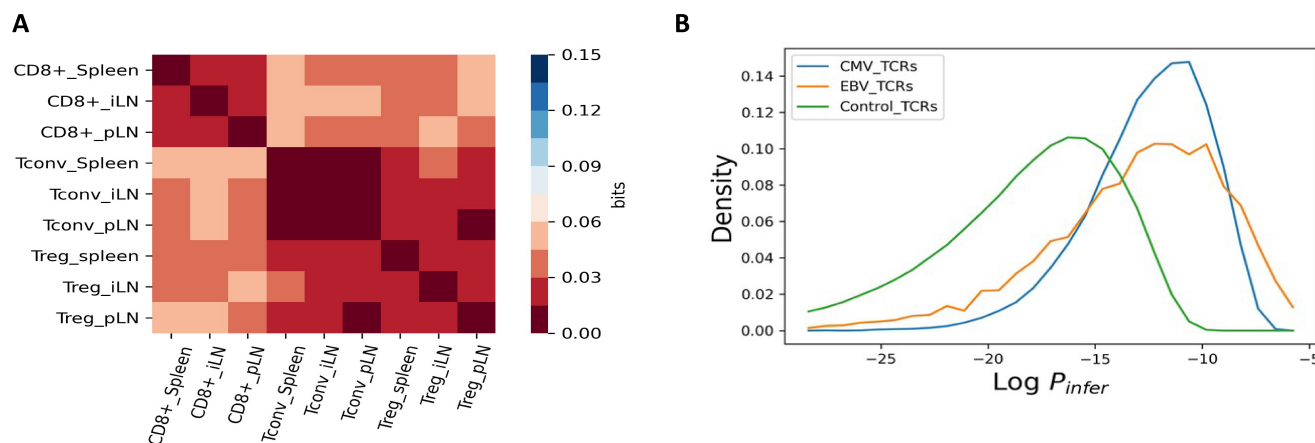


Figure 3. (A) Jensen-Shannon divergences between TCR subrepertoires at the cell type and tissue level. Jensen-Shannon divergences (D_{JS}) were computed from TCRpeg trained on different subrepertoires (Methods). (B) Density map of inferred logarithmic probabilities for the three repertoires according to the TCRpeg model. For each repertoire, we inferred a TCRpeg model.

1 TCRpeg helps profile TCR repertoires

2 The learned probability distribution can help profile the TCR subrepertoires in a probabilistic manner. Here,
3 we were interested in learning the cell-type-level discrepancy and exploring the tissue-level differences
4 since T-cells migrate and reside in different tissues and are influenced by different tissue environments.
5 During maturation in the thymus, T-cells are selected and differentiate into two major cell types: cytotoxic
6 ($CD8^+$) and helper ($CD4^+$) T-cells which function differently. Thus, our aim was to explore the TCR
7 preferences of different TCR subrepertoires. To collect the data, we pooled TCRs with unique nucleotide
8 sequences from nine healthy individuals from Seay *et al.*²¹. These TCR sequences were classified into
9 three cell types ($CD4^+$ conventional T-cells [Tconvs], $CD4^+$ regulatory T-cells [Tregs], and $CD8^+$ T-
10 cells) and collected from three tissues (pancreatic draining lymph nodes [pLNs], mesenteric or inguinal
11 “irrelevant” lymph nodes [iLNs], and spleen); that is, we have nine classes of subrepertoires. We applied
12 TCRpeg to infer the probability distribution of each subrepertoire and quantified the difference between
13 these distributions using the Jensen-Shannon divergence D_{JS} (Methods).

14 We observed that the subrepertoires belonging to the same cell type are more conserved across different
15 tissues. The same cell type in different tissues shows a lower TCR subrepertoire divergence, with an
16 average Jensen-Shannon divergence as $D_{JS} \simeq 0.014$ bits (Fig. 3A). However, the divergence is high
17 between $CD8^+$ and $CD4^+$ TCR subrepertoires with the average $D_{JS} \simeq 0.041$ bits. Tconv and Treg
18 within the class of $CD4^+$ cells demonstrate moderate similarities, with average $D_{JS} \simeq 0.024$ bits. These

1 observations confirm the results from Isacchini *et al.*¹⁹, where larger divergence between the CD8⁺ and
2 CD4⁺ TCR subrepertoires and lower difference between the Tconv and Treg TCR subrepertoires are
3 shown. These results were as expected since the CD8⁺ and CD4⁺ T-cells function significantly different:
4 CD4⁺ T-cells are MHC-II restricted and pre-programmed for helper functions, whereas CD8⁺ T-cells
5 are MHC I-restricted and pre-programmed for cytotoxic functions⁴⁰. Additionally, subrepertoires of
6 different tissues showed minor divergence, indicating that subsets of T cells perform similar functions
7 across tissues.

8 Next, we profiled two infection-specific TCR repertoires to further validate TCRpeg. We collected
9 TCRs associated with cytomegalovirus (CMV) and Epstein-Barr virus (EBV) from VDJdb⁴¹ with 18,560
10 and 4,350 sequences, respectively. Furthermore, we randomly sampled 10^6 TCRs from the aforementioned
11 universal TCR pool as control. Figure 3B illustrates the density map of inferred probabilities for each
12 repertoire. As expected, each repertoire had a distinct probability distribution. We then used a simple
13 classifier to further show the characterization capacity of TCRpeg. We first trained a TCRpeg model
14 for each repertoire. Then, we assigned a TCR x to the group r if $P_r(\mathbf{x}) > P_{r'}(\mathbf{x})$, and vice versa, where
15 r and r' are two repertoires. Interestingly, we observed an average accuracy 0.791 for classifying
16 CMV-associated TCRs from control and 0.801 for classifying EBV-associated TCRs with a 5-fold cross-
17 validation procedure.

18 **Classification of cancer-associated TCRs and SARS-CoV-2 epitope-specific TCRs**

19 TCRpeg yields vector embeddings for TCRs sequences. Compared to the predefined or manually designed
20 encoding method for TCR sequences, TCRpeg provides a learnable way to encode TCR sequences into
21 vector representations. The update and reset gates of the GRU layers are learned during the training
22 process to determine how much of the previous information stored in the hidden features needs to be
23 passed along or abandoned²⁶ (Fig. 1A). Therefore, the hidden features of the GRU layers at the last
24 sequence position store summative information of the TCR sequences with different lengths; and these
25 feature vectors provide an embedding for the TCR sequences.

26 To illustrate the embedding of the TCR sequence, we first collected cancer-associated TCR (caTCR)
27 from Beshnova *et al.*¹⁷ ($N \sim 43,000$) and SARS-CoV-2 epitope (YLQPRTFL) specific TCRs from VDJdb

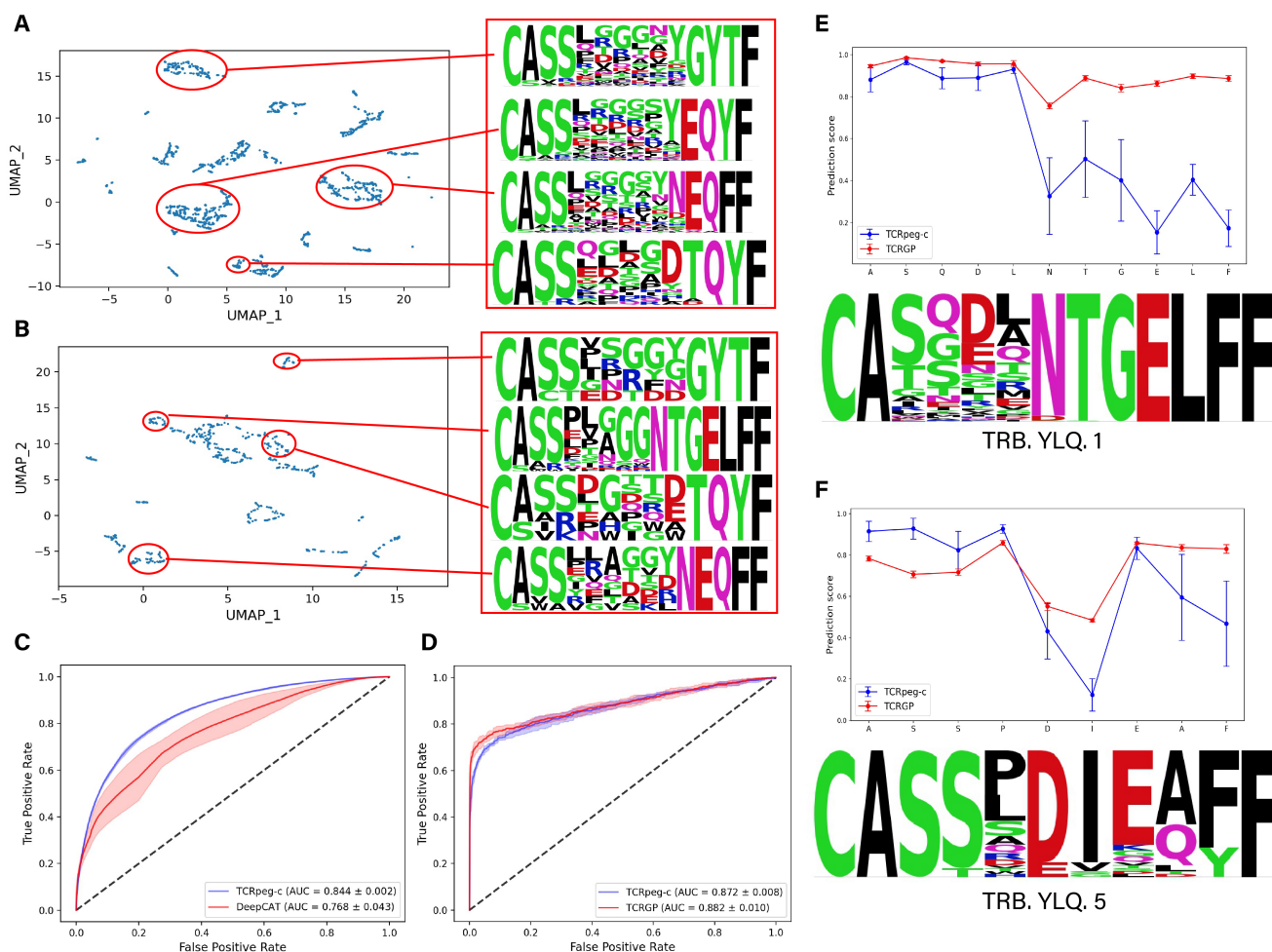


Figure 4. 2D illustration of TCRpeg-based encodings and predictive performance for downstream classification tasks. (A and B) 2D projection map of encodings obtained from TCRpeg trained on (A) caTCRs and (B) specific TCRs of the SARS-CoV-2 epitope (YLQPRTFLL). More projecting results can be found in Supplementary S3. (C and D) ROC curves for tasks of (C) predicting caTCR and (D) SARS-CoV-2 epitope YLQPRTFLL. (E and F) Sensitivity analysis through amino acid substitutions used TCRpeg-c and TCRGP for two previously identified TCR motifs. For each position other than the two ends, we changed the amino acid at that position to the four other most frequent AAs and used these two models to score the modified sequences. TCRpeg-c is more sensitive than TCRGP to substitutions of amino acids inside the motifs.

1 database⁴¹ (N=683). We trained TCRpeg on these two datasets separately and obtained the respective
2 numerical TCR embedding vectors. The UMAP dimensionality reduction⁴² was applied to project these
3 vectors onto 2D space (Fig. 4A, Fig. 4B and Supplementary S3), showing that TCRs with a similar
4 pattern (motif) tend to be clustered. It implies that the encodings could be helpful for antigen-specific TCR
5 clustering. To further demonstrate the utility of TCRpeg-based encodings, we evaluated the classification
6 performance on caTCRs and SARS-COV-2-epitope-specific TCRs using a fully connected neural network
7 (FCN), taking these vector encodings as input. Since TCRpeg was designed mainly for TCR β chain
8 and the paired TCR α and β chain are scarce, in this section we aimed mainly to investigate predictive
9 performance with respect to TCR β sequences. We refer to this network as “TCRpeg-c” (Methods and

1 Supplementary S4). To collect negative (or control) samples for the epitope-specific TCR dataset, we
2 randomly sampled ten times more negative data than positive data from the universal repertoire of TCR
3 mentioned above. We selected the CNN-based model, DeepCAT, developed in Beshnova *et al.* to compare
4 with the caTCR prediction task, adopting the five-fold cross-validation procedure. In this prediction task,
5 we observed an improvement in accuracy and predictive stability for TCRpeg-c with an average AUC
6 $\simeq 0.844$ compared to DeepCAT with an average AUC $\simeq 0.768$ of caTCRs (Fig. 4C).

7 In the more challenging epitope-specific TCR prediction task with scant data, TCRpeg-c still demon-
8 strated competitive performance with AUC $\simeq 0.872$ compared to the baseline method TCRGP²⁷ with
9 AUC $\simeq 0.882$ (Fig. 4D). However, the TCRGP model is sophisticated, and it is designed specifically for
10 the TCR-epitope mapping problem with low data size, combining multiple techniques including alignment
11 of TCR sequences, Gaussian process (GP) and variational inference.

12 TCRpeg-c finds TCR motifs through perturbation analysis. TCR motifs are important and instructive
13 in determining their specificity to antigens⁴³. Previously, motif discovery for TCR repertoires was
14 mainly accomplished by exploring similarities between TCRs such as the TCRNET method^{44–46} or
15 investigation of frequency enhancement of k-mers for TCRs⁴³. Here, we used predictive models to
16 test the sensitivity of previously identified TCR motifs for specific TCRs of the SARS-CoV-2 epitope
17 YLQPRTFLL (Methods). We observed the correspondence between previously identified TCR motifs and
18 sensitive residues according to the TCRpeg-c predicted scores, indicating the importance of TCR motifs
19 for epitope binding (Fig. 4E and 4F). However, although TCRGP achieves high predictive performance, it
20 lacks the ability to detect sensitive residues (Fig. 4E and 4F). We attribute its insensitivity to the need to
21 pad TCR sequences to a fixed length, which could lower the degree of variation caused by amino acid
22 substitution.

23 **Generating more TCR sequences with potentially the same specificity**

24 A good generative model could be beneficial for the adoptive transfer of TCR engineered T-cells (TCR-T)
25 that has been applied to treat viral infections such as hepatitis B and C^{47,48}, cancer immunotherapy^{49,50},
26 and autoimmune disease therapy⁵¹ through *in silico* generation of similar TCR sequences guiding the *in*
27 *vitro* TCR design. We extended TCRpeg to be generative through a simple sampling strategy (Methods).

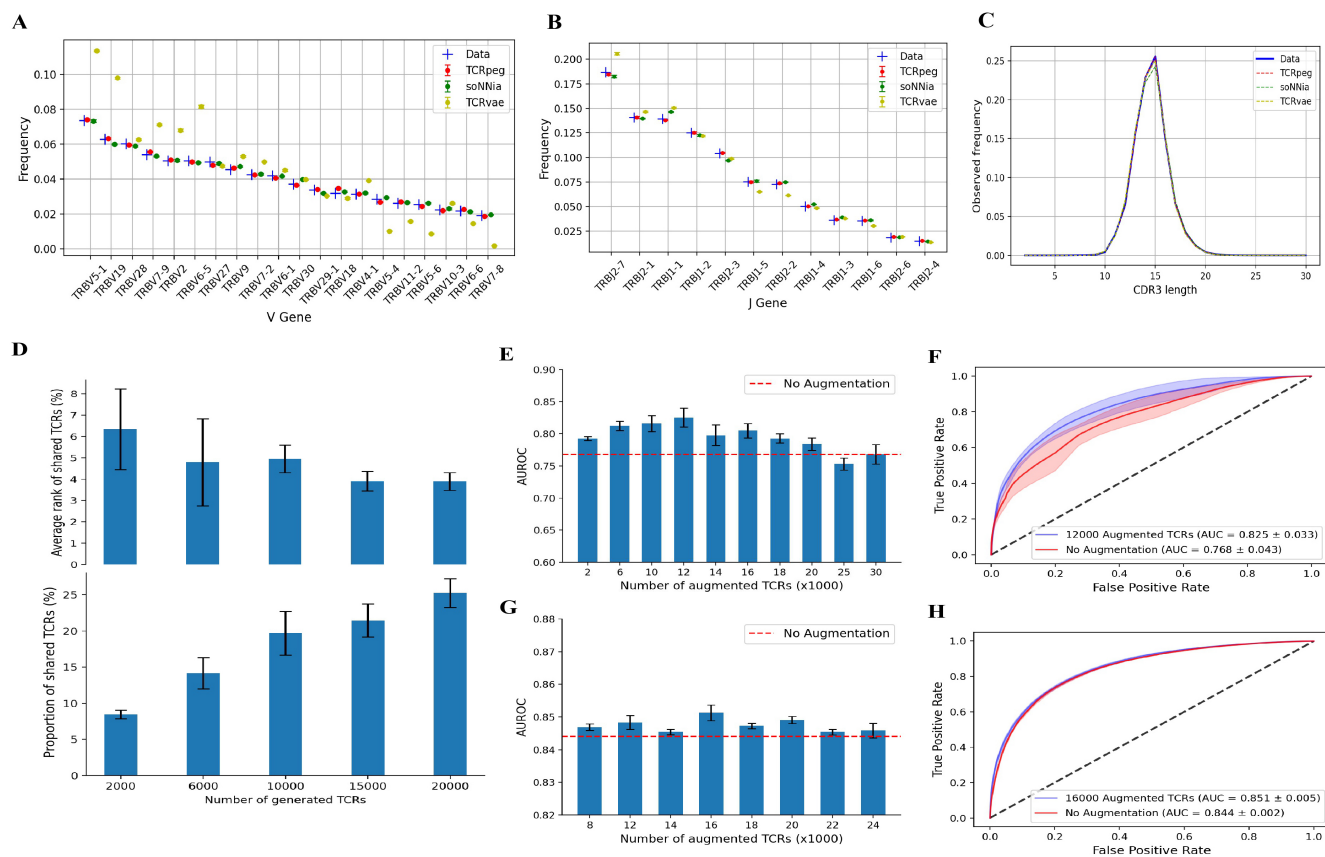


Figure 5. Characteristics of the TCR sequences generated by the three generative models. (A-C) Comparison of the statistical distributions of the generated sequences with the real data with respect to (A) V gene usage, (B) J gene usage and (C) length distribution. In (A), only the top 20 frequent V genes are listed. We include the figure of full V gene usage and the distributions of amino acids in Supplementary S7 and S6. (D) The proportion of the TCR sequences in the test set that also appears in the generated TCRs (bottom panel) and the average probability rank of those shared TCRs among the generated TCRs (top panel).

With more TCRs being generated, more of them can be found in the test set. (E - H) Performance in the task of predicting caTCRs by applying the TCR-specific data augmentation technique. (D and F) The AUC scores with a different number of augmented TCR sequences when using the (E) DeepCAT model and (G) TCRpeg-c. (F and H) ROC curves for the DeepCAT model (E) and TCRpeg-c (G) with the best number of augmented TCRs.

1 We first aimed to systematically evaluate and compare the generation ability of TCRpeg with the
 2 baseline methods, soNNia and TCRvae, in terms of the statistical properties between the generated
 3 TCR sequences and real sequences. Specifically, we investigated the distributions of sequence lengths,
 4 positions of amino acids, V gene and J gene usages. We observed strong agreement between the probability
 5 distributions of *in silico* and real TCR repertoires for both the TCRpeg and soNNia models. For the position
 6 distributions of each amino acid, the TCRpeg- and soNNia- generated sequences successfully fitted the
 7 original statistics with an average Pearson correlation coefficient $r \simeq 1.0$ and $r \simeq 0.999$, respectively,
 8 compared to TCRvae with $r \simeq 0.982$ (Supplementary S6). For V and J gene usages, the TCRpeg
 9 and soNNia models still outperform TCRvae, achieving average $r \simeq 0.999$ and $r \simeq 0.998$ compared to
 10 $r \simeq 0.949$ of the TCRvae model for V gene usage distribution (Fig. 5A and Supplementary S7), and

1 $r \simeq 1.0$ and $r \simeq 0.997$ over $r \simeq 0.993$ for J gene usage distribution (Fig. 5B). For the length distribution,
2 these three models all achieved highly accurate performance with $r \simeq 1.0, 0.998, 1.0$ for TCRpeg, soNNia,
3 and TCRvae, respectively (Fig. 5C). The generation performance of TCRpeg is stable and accurate even
4 when trained on a small subset of TCRs (Supplementary S8 and S9). These results together highlight that
5 TCRpeg is reliable for summarizing a TCR repertoire, and consequently, generating new sequences in
6 recovering the real statistical distributions.

7 A reliable generative model should be able to produce new TCR sequences with “hidden similarity”
8 to real TCR data, in addition to statistical similarity. Here, we were interested to determine whether the
9 generated TCR sequences possess the same epitope specificity with the data used in training TCRpeg. To
10 verify this, we retrained TCRpeg on the training set of the TCRs specific to the epitope YLQPRTFL
11 and utilized it to generate new sequences accordingly. We first noticed that some of the TCRs in the
12 test set could also be found in the generated data set (Fig. 5D), which shows the generative power of
13 TCRpeg given the wide potential diversity of TCR sequences. To take a closer look at these generated
14 TCR sequences, we observed that those TCRs that were also found in test set possessed high generation
15 probabilities (averagely ranked $< 10\%$ among generated sequences, Fig. 5D). Finally, we utilized the
16 TCRMatch²⁸ software to further validate the hidden similarity of the generated TCR sequences and
17 observed that 50 – 60% of them possess the same epitope specificity as the TCR sequences used in training
18 according to a scoring threshold of 0.9 (Supplementary S10). On the contrary, although the soNNia and
19 TCRvae models achieve comparable performance with respect to statistical similarities, only less than 40%
20 of the generated sequences possess the same epitope specificity determined by the same scoring threshold
21 (Supplementary S10). Overall, our results indicate that TCRpeg can generate new TCR sequences with
22 statistical and possible hidden similarities to the TCRs used for training.

23 **Augmenting TCR sequencing data**

24 Data augmentation techniques are ubiquitously used in machine learning tasks to increase the generality
25 of data by adding similar samples generated by either slightly modifying the original data or synthesizing
26 similar data. They act as regularizers to alleviate the issue of overfitting and improve the generalization ca-
27 pacity of machine learning models, especially when applied to computer vision tasks⁵² or natural language

1 processing tasks⁵³. Adopting the data augmentation techniques here should improve the classification
2 of TCR sequences. TCR sequences might abolish their epitope specificity by amino acid substitutions,
3 especially when they happen inside contact motifs^{43,54}; therefore, directly performing amino acid substitu-
4 tions, insertions, or deletions on TCR sequences cannot work as data augmentation. However, with strong
5 generative ability, TCRpeg may generate similar TCR sequences and serve as a computational tool for
6 TCR-specific data augmentation.

7 To analyze the feasibility of TCR-specific data augmentation, we evaluated and compared the predictive
8 performance of classifying caTCRs with and without data augmentation while keeping all other training
9 settings unchanged. For the DeepCAT model, we observe a large performance gain with up to 0.057
10 higher AUC when applying data augmentation technique (Fig. 5E and 5F). For the TCRpeg-c model,
11 we still find accuracy enhancement in the AUC value from 0.844 to 0.851 with data augmentation (Fig.
12 5G and 5H). Besides, the AUPRC (area under the precision-recall curve) also increases and the test loss
13 decreases, which is a positive sign of mitigation of overfitting (Supplementary S11). To further validate
14 the utility of our TCRpeg-based augmentation technique, we performed classification for the influenza
15 epitope GILGFVFTL and EBV epitope GLCTLVAML specific TCRs with 3,406 and 962 positive samples,
16 respectively, using the TCRex model⁵⁵. Without changing any training settings, we observed up to 2.1%
17 and 21.4% accuracy enhancement for these two TCR datasets (Supplementary S12).

18 Discussion

19 An accurate probabilistic model for large-scale TCR sequencing data is a cornerstone for a better un-
20 derstanding of functional TCR repertoire. Previous works have developed selection models soNia²⁵,
21 soNNia¹⁹, and the VAE-based model TCRvae²⁹ to characterize the distribution of productive TCR se-
22 quences. However, they are all intrinsically unable to capture the information behind the length variation.
23 In this work, we introduced TCRpeg, an autoregressive deep learning model that utilizes a recurrent neural
24 network with GRU layers to characterize the TCR repertoires. Unlike soNia, soNNia, and TCRvae which
25 need to pad every TCR sequence to the same length, TCRpeg can process TCR sequences with any lengths.
26 Such capability can eliminate the noise introduced by adding an extra “amino acid” for padding and take
27 advantage of the information behind the variance in lengths.

1 We first demonstrated that TCRpeg can improve the statistical characterization of TCR repertoires in
2 a large cohort of individuals³⁹ compared to soNNia and TCRvae by a large margin, which implies that
3 TCRpeg can better learn the TCR sequence pattern. We attribute the superior performance of TCRpeg
4 to its ability to process TCRs with different lengths and its transmission of hidden features that properly
5 store the previous information. In particular, TCRpeg takes less iterations to converge and requires lower
6 computation resources. These results indicate the advantages of using an autoregressive model that is
7 capable of processing TCR sequences with different lengths to describe large-scale TCR sequencing data
8 from a probabilistic perspective.

9 Using the statistical inference power of TCRpeg, we explored the differences and similarities between
10 functional TCR subrepertoires collected from different T-cell types or tissues at the repertoire level. We
11 discovered that TCR subrepertoires belonging to families with more closely related developmental paths
12 (i.e., Tconvs and Tregs) possess higher statistical similarities. Meanwhile, they both show large differences
13 with CD8⁺ T-cells that diverged earlier in T-cell maturation. Next, we explored the statistical profile of the
14 infection-specific TCR repertoires and observed their distinct patterns through the density map (Fig. 3B).
15 To illustrate the characterization capacity of TCRpeg in a more straightforward way, we used a simple
16 classifier that directly applied the probability inference ability of TCRpeg to classify the infection-specific
17 TCRs. This simple classifier achieved relatively high prediction performance, with an average accuracy
18 of 0.791 for classifying CMV and 0.801 for classifying EBV associated TCRs. Our results showed that
19 TCRpeg is a superior tool for characterizing TCR repertoires from a statistical perspective.

20 On the basis of the architecture of TCRpeg, we can obtain helpful vector representations of TCR
21 sequences from the trained TCRpeg model, which is not provided by soNNia or TCRvae. Compared to
22 other predefined or hand-designed encoding methods for TCR sequences, TCRpeg provides a learnable
23 way to encode TCR sequences by updating functional gates inside GRU layers²⁶. We observed that
24 TCRpeg-based TCR encodings could reflect the degrees of similarities between TCR sequences that
25 sequences with a similar pattern (motifs) tend to cluster together (Fig. 4A and 4B). This suggests a
26 potential application of antigen-specific TCR clustering, since shared TCR motifs indicate the same
27 antigen specificity.

28 To examine the performance of TCRpeg-based encodings in a predictive manner, we assessed the

1 classification performance of caTCRs and YLQPRTFLL epitope-specific TCRs using a fully connected
2 neural network taking these vector encodings as input (TCRpeg-c). For the caTCR prediction task, we
3 chose the DeepCAT model developed by Beshnova *et al.* as the baseline method. We observed a significant
4 improvement in accuracy and predictive stability for TCRpeg-c compared to DeepCAT in the prediction
5 of caTCRs (Fig. 4C). With such high precision, TCRpeg-c could facilitate cancer detection through the
6 process introduced in Beshnova *et al.*. In recent years, multiple machine learning methods have been
7 developed to predict the epitope specificity of TCRs, such as TCRex⁵⁵, DeepTCR⁵⁴, and TCRGP²⁷. All of
8 these methods have explored the problem in slightly different settings and compared with each other. In the
9 more challenging classification task of predicting SARS-CoV-2 epitope (YLQPRTFLL)-specific TCRs, we
10 compared TCRpeg-c to a representative of the above group of machine learning models, TCRGP, which is
11 a combination of multiple functional modules including TCR alignment, Gaussian process, and variational
12 inference. TCRpeg-c demonstrated competitive performance in this task compared to TCRGP (Fig. 4D).
13 In particular, TCRpeg-c is sensitive to substituting for an amino acid primarily when it occurs inside the
14 TCR motifs, while TCRGP is insensitive to that (Fig. 4E and 5F). This finding indicates that TCRpeg-c
15 can be used for motif validation and help with TCR engineering for immunotherapies⁵⁶. In addition, this
16 perturbation analysis might reveal *de novo* motifs that have not yet been discovered using nonpredictive
17 methods (Supplementary S5). The comparable accuracy performances in the above two classification
18 challenges validate the advantage of TCRpeg-based encodings, which can be further concatenated with
19 epitope features to facilitate the unseen epitope-TCR interaction prediction task⁵⁷.

20 One direct application of TCRpeg is to generate new TCR sequences with characteristics similar to
21 those of natural sequences. We first compared the generation capability of TCRpeg with soNnia and
22 TCRvae with respect to the statistical distributions on the large universal TCR pool we have constructed.
23 We showed that TCRpeg-generated TCR sequences had the closest amino acid distributions, length
24 distribution, and V/J gene usages to the real sequences compared to the other baseline methods. Next,
25 we found that some TCRs in the test set could also be found in the generated dataset, and those shared
26 TCRs have high generation probabilities among the generated dataset (Fig. 5D). These results imply that
27 newly generated TCR sequences with high probabilities might share the same epitope specificity with the
28 data used in training, providing a potential way to meet the demand for more data. We further applied the

1 TCRMatch²⁸ software to validate this implication and show that 50 – 60% of the generated TCRs share
2 the same epitope specificity as the TCRs used for training. On the contrary, less than 40% of the TCRs
3 generated using TCRvae or soNNia share the same specificity (Supplementary S10). The generative power
4 of TCRpeg can also be used to design similar TCRs to facilitate immunotherapy for T-cell transfer^{49–51}.

5 Data augmentation is a ubiquitous technique used to increase the performance of machine learning
6 models, especially in computer vision systems⁵². Given that more and more machine learning models
7 have been developed for TCR-related tasks and the acquisition of more data is costly and time consuming,
8 which restricts the development of highly accurate machine learning models, we developed and validated
9 the TCR-specific data augmentation technique empowered by TCRpeg to relieve such restriction. For the
10 caTCR classification task, we observed a notable improvement with data augmentation (Fig. 5E and 5F).
11 In addition, we further validated the utility of data augmentation using another machine learning model -
12 TCRex⁵⁵ in the prediction tasks of GILGFVFTL and GLCTLVAML specific TCRs and again observed an
13 improvement in accuracy (Supplementary S12). However, in the SARS-CoV-2 specific TCR recognition
14 task, data augmentation failed to boost the model performance. When learning from such a small data size,
15 TCRpeg tends to generate highly similar TCRs with those in the training set and thus provides limited
16 additional information to the predictive model, which might result in more severe overfitting. Nevertheless,
17 TCRpeg-based data augmentation is a free option for boosting model performance without any extra cost.

18 In this work, we have introduced a new holistic software tool TCRpeg for estimating the probability
19 distribution of a TCR repertoire with a great performance enhancement over previous works. Furthermore,
20 with promising performance in probability inference, TCRpeg improves on a range of TCR-related tasks:
21 (i) reveal TCR repertoire-level discrepancies from a probabilistic prospective; (ii) classify antigen-specific
22 TCRs and validate previously discovered TCR binding motifs; (iii) generate novel TCRs and augment
23 TCR data for accuracy enhancement of machine learning models. Our results and analysis highlight
24 the flexibility and capacity of TCRpeg to extract TCR sequence information, providing new insights for
25 understanding the complex genomic concepts hidden behind TCR repertoires.

1 **Methods**

2 **Data Description**

3 The data sets used in this work are classified into three groups to evaluate the performance of TCRpeg. We
4 filter out TCRs with lengths greater than 30 or not starting with a cysteine in all data sets. We also verified
5 sequences that are written as V gene, CDR3 sequence, J gene and removed sequences with unknown
6 genes. In addition, we only considered the 20 standard amino acids in this work and removed sequences
7 with any unspecified amino acid. The detailed descriptions of each group of data are shown below:

- 8 1. To quantify the precision of the inference of TCRpeg along with the other two baseline methods, we
9 used the TCR repertoires sampled from a large cohort, including 743 individuals from Emerson
10 *et al.*³⁹ We pooled the unique nucleotide sequences of receptors from all individuals and built a
11 universal TCR pool that contains around 10^9 sequences in total. The multiplicity of an amino acid
12 sequence in this universal TCR pool indicates the number of independent recombination events that
13 led to that receptor. We randomly and equally split the TCR pool into a training set and a test set.
- 14 2. To characterize the differences between the TCR subrepertoires of functional cell types collected
15 from different tissues, we pooled unique TCRs from 9 control donors from Seay *et al.*²¹ at the tissue
16 level. These TCR sequences were sorted into three cell types and collected from three tissues. Thus,
17 for each donor status (healthy or T1D), we have nine groups of TCRs. Again, the multiplicity of an
18 amino acid sequence in this universal TCR pool indicates the number of independent recombination
19 events that led to that receptor, which is used to calculate the real probability distribution.
- 20 3. To evaluate the performance of TCRpeg-c in classification tasks, we first collected cancer-associated
21 TCRs (caTCRs) from Beshnova *et al.*¹⁷. Briefly, Beshnova and his colleagues collected TCR
22 sequences from approximately 4,200 recorded samples downloaded from The Cancer Genome
23 Atlas (TCGA) and excluded those sequences that are also found in healthy donors. The remaining
24 around 43000 TCR sequences are assumed to be cancer-associated TCRs (caTCRs). We extracted
25 the SARS-CoV-2 epitope (YLQPRTFLL), influenza epitope GILGFVFTL and EBV GLCTLVAML
26 specific TCRs from VDJdb⁴¹ database (positive TCRs N = 683, 3406, 962, respectively, extracted

1 on 24 January 2022). We then randomly sampled ten times more negative data than positive data
2 from the universal TCR pool constructed previously to serve as the control TCRs.

3 **TCRpeg and TCRpeg-c**

4 The illustrations of TCRpeg and TCRpeg-c are shown in Fig. 1A and Supplementary S4. To enable the
5 training of TCRpeg, we first trained the word2vec³⁸ model on 1×10^6 TCR sequences randomly sampled
6 from the pooled universal repertoire aforementioned to obtain the numerical embeddings for each amino
7 acid, regarding the amino acid as the “words” and the TCR sequences as the “sentences”. Specifically,
8 we adopted the skip-gram architecture with the window size and embedding size set to 2 and 32 and
9 trained it for 20 epochs. For the TCRpeg model, the GRU modules have three layers with the size of the
10 hidden feature set to 64. We trained TCRpeg using the Adam⁵⁸ optimizer for 20 epochs to minimize the
11 cross-entropy loss between the soft-maxed logits and the one-hot encoded representation of the discrete
12 categorical outputs of the network. The probability of a given TCR sequence $P_{infer}(\mathbf{x})$ is estimated using
13 Equation 1. Specifically, we input the given TCR sequence to TCRpeg and obtain the corresponding
14 output probability distribution of the amino acid at the next time step. Thus, $P_{infer}(\mathbf{x})$ is the multiplication
15 of the probabilities of amino acids at each time step.

16 For the TCRpeg-c model, the size of the hidden feature is increased to 512 to better capture the hidden
17 sequence features for classification tasks. On top of the pre-trained TCRpeg, the fully connected neural
18 network contains two hidden layers with 384 and 96 neurons, followed by the ReLU activation function.
19 In the task of predicting caTCRs, we trained TCRpeg-c for 30 epochs to minimize the loss of cross-entropy
20 between the output logits and true labels, with dropout operations ($p=0.2$) to reduce the issue of overfitting.
21 In classifying epitope-specific SARS-CoV-2 TCRs, we trained TCRpeg-c for 20 epochs with a dropout
22 rate set to 0.4. In both above-mentioned classification tasks, the TCRpeg was trained on the respective
23 training set to provide the numerical embeddings for TCRs. The trained TCRpeg-c can be used to find
24 TCR motifs through perturbation analysis. Specifically, we permuted each position of the TCR sequences
25 except for the first and last positions, with four other amino acids that most likely appeared at that position
26 according to the amino acid frequency at that position. We adopted this strategy to avoid skewed permuted
27 sequences containing amino acids at some positions with nearly zero probabilities. We then applied the

1 trained TCRpeg-c to score each permuted sequence to determine residues that are sensitive to changes.

2 **Quantifying the accuracy of probability inference.**

3 To evaluate the precision of probability inference, we compared the estimated probabilities $P_{infer}(\mathbf{x})$ to
4 the observed frequencies $P_{data}(\mathbf{x})$ of the test set. The accuracy can be quantified by Pearson's correlation
5 coefficient r between $P_{infer}(\mathbf{x})$ and $P_{data}(\mathbf{x})$. A higher value of r indicates a better model. The calculation
6 of $P_{infer}(\mathbf{x})$ for TCRpeg is described in the previous section using the autoregressive likelihood formula.
7 For the two baseline methods TCRvae and soNNia, we compute $P_{infer}(\mathbf{x})$ by:

$$P_{infer}(\mathbf{x}) = \sum_{v,j} P_{infer}(\mathbf{x}, v, j), \quad (2)$$

8 which sums the V and J genes along with the TCR sequence \mathbf{x} . Finally, we normalize the inferred
9 probabilities $P_{infer}(\mathbf{x})$ and consider them as the approximation of the real probability distribution.

10 **Quantifying of difference between TCR subrepertoires**

11 We used the Jensen-Shannon divergence $D_{JS}(r^i, r^j)$ to characterize the difference between two TCR
12 subrepertoires r^i and r^j :

$$D_{JS}(r^i, r^j) = \frac{1}{2}D_{KL}(P_{infer}^i, M) + \frac{1}{2}D_{KL}(P_{infer}^j, M), \quad (3)$$

13 where P_{infer}^i and P_{infer}^j are computed by two different TCRpeg separately trained on subrepertoires r^i
14 and r^j , $M = \frac{1}{2}(P_{infer}^i + P_{infer}^j)$ and D_{KL} represent the Kullback-Leibler divergence. To characterize the
15 differences between the TCR subrepertoires of functional cell types collected from different tissues, we
16 first trained TCRpeg on each tissue-level TCR subset for 20 epochs with hidden size and the number of
17 layers set to 128 and 3, respectively. Then we applied Eq. 3 to calculate the JS divergences between each
18 pair of those TCR subrepertoires.

19 **Using TCRpeg to generate TCR sequences**

20 We adopted a simple sampling method to generate new TCR sequences using TCRpeg. Specifically, we
21 first input the start token (“<SOS>”) to the TCRpeg and then randomly sampled the amino acid for the

1 next position from the output probability distribution (computed using the Softmax operation). Following
2 the same procedure, at each time step, we randomly sampled the amino acid for that time step according to
3 the probability distribution defined by the predicted scores and input it to the next time step to obtain the
4 following amino acids. This stochastic generation procedure can be described by the formula stated below:

$$AA_t = P(AA|AA_{t-1:0}; \boldsymbol{\theta}), \quad (4)$$

5 where AA_0 stands for the start token and $\boldsymbol{\theta}$ represents the TCRpeg parameters. The generation process
6 stops when the special stop token (“<EOS>”) is generated. To allow the ability to infer the corresponding
7 V and J gene along with the TCR sequence, we extended TCRpeg and formulated the probability of a
8 given TCR sequence \mathbf{x} with specific V and J genes as:

$$p(\mathbf{x}, V, J | \boldsymbol{\theta}_1, \boldsymbol{\theta}_2, \boldsymbol{\theta}_3) = p(x_1 | \boldsymbol{\theta}_1) \prod_{i=2}^L p(x_i | x_1, \dots, x_{i-1}; \boldsymbol{\theta}_1) p(V | \mathbf{x}; \boldsymbol{\theta}_2) p(J | \mathbf{x}; \boldsymbol{\theta}_3), \quad (5)$$

9 where $p(V | \mathbf{x}; \boldsymbol{\theta}_2)$ and $p(J | \mathbf{x}; \boldsymbol{\theta}_3)$ are the probabilities conditioning on the TCR sequence \mathbf{x} ; $\boldsymbol{\theta}_2$ and $\boldsymbol{\theta}_3$ are
10 parameterized by two respective fully connected single-layer neural networks. The TCRpeg, soNNia and
11 TCRvae models were inferred from the universal TCR repertoire aforementioned, and then we applied
12 them to generate new TCR sequences along with V and J genes.

13 **Availability of data and materials**

14 All data analyzed in this work can be found in the original publications that collected the data^{17,21,39,41}, and
15 we include the preprocessed data at <https://github.com/jiangdada1221/TCRpeg#data>.
16 TCRpeg was written in Python using the deep learning library Pytorch⁵⁹ and is available as a python
17 package. Source code, use-case tutorials, and documentations can be found at [https://github.com/](https://github.com/jiangdada1221/TCRpeg)
18 [jiangdada1221/TCRpeg](https://github.com/jiangdada1221/TCRpeg). Users can install directly from Github or PyPI via pip.

1 **Funding**

2 This work was supported by strategic interdisciplinary research grant [7005215] from the City University
3 of Hong Kong.

4 ***Conflict of interest statement.***

5 None declared.

6 **References**

- 7 **1.** Susumu Tonegawa. Somatic generation of antibody diversity. *Nature*, 302(5909):575–581, 1983.
- 8 **2.** Mark M Davis and Pamela J Bjorkman. T-cell antigen receptor genes and t-cell recognition. *Nature*,
9 334(6181):395–402, 1988.
- 10 **3.** Srinika Ranasinghe, Pedro A Lamothe, Damien Z Soghoian, Samuel W Kazer, Michael B Cole,
11 Alex K Shalek, Nir Yosef, R Brad Jones, Faith Donaghey, Chioma Nwonu, et al. Antiviral cd8+ t cells
12 restricted by human leukocyte antigen class ii exist during natural hiv infection and exhibit clonal
13 expansion. *Immunity*, 45(4):917–930, 2016.
- 14 **4.** P Anton Van Der Merwe and Omer Dushek. Mechanisms for t cell receptor triggering. *Nature*
15 *Reviews Immunology*, 11(1):47–55, 2011.
- 16 **5.** Philippa Marrack and John Kappler. The t cell receptor. *Science*, 238(4830):1073–1079, 1987.
- 17 **6.** Jannie Borst, Heinz Jacobs, and Gaby Brouns. Composition and function of t-cell receptor and b-cell
18 receptor complexes on precursor lymphocytes. *Current opinion in immunology*, 8(2):181–190, 1996.
- 19 **7.** Nishant K Singh, Timothy P Riley, Sarah Catherine B Baker, Tyler Borrman, Zhiping Weng, and
20 Brian M Baker. Emerging concepts in tcr specificity: rationalizing and (maybe) predicting outcomes.
21 *The Journal of Immunology*, 199(7):2203–2213, 2017.
- 22 **8.** XL Hou, L Wang, YL Ding, Q Xie, and HY Diao. Current status and recent advances of next
23 generation sequencing techniques in immunological repertoire. *Genes & Immunity*, 17(3):153–164,
24 2016.

- 1 **9.** Sebastian Zeissig, Elisa Rosati, C Marie Dowds, Konrad Aden, Johannes Bethge, Berenice Schulte,
2 Wei Hung Pan, Neha Mishra, Maaz Zuhayra, Marlies Marx, et al. Vedolizumab is associated with
3 changes in innate rather than adaptive immunity in patients with inflammatory bowel disease. *Gut*,
4 68(1):25–39, 2019.
- 5 **10.** Jonathan R McDaniel, Brandon J DeKosky, Hidetaka Tanno, Andrew D Ellington, and George
6 Georgiou. Ultra-high-throughput sequencing of the immune receptor repertoire from millions of
7 lymphocytes. *Nature protocols*, 11(3):429–442, 2016.
- 8 **11.** Maria A Turchaninova, Olga V Britanova, Dmitriy A Bolotin, Mikhail Shugay, Ekaterina V Putintseva,
9 Dmitriy B Staroverov, George Sharonov, Dmitriy Shcherbo, Ivan V Zvyagin, Ilgar Z Mamedov, et al.
10 Pairing of t-cell receptor chains via emulsion pcr. *European journal of immunology*, 43(9):2507–2515,
11 2013.
- 12 **12.** Pradyot Dash, Andrew J Fiore-Gartland, Tomer Hertz, George C Wang, Shalini Sharma, Aisha
13 Souquette, Jeremy Chase Crawford, E Bridie Clemens, Thi HO Nguyen, Katherine Kedzierska,
14 et al. Quantifiable predictive features define epitope-specific t cell receptor repertoires. *Nature*,
15 547(7661):89–93, 2017.
- 16 **13.** David Masopust and Louis J Picker. Hidden memories: frontline memory t cells and early pathogen
17 interception. *The Journal of Immunology*, 188(12):5811–5817, 2012.
- 18 **14.** Nina Le Bert, Anthony T Tan, Kamini Kunasegaran, Christine YL Tham, Morteza Hafezi, Adeline
19 Chia, Melissa Hui Yen Chng, Meiyin Lin, Nicole Tan, Martin Linster, et al. Sars-cov-2-specific t cell
20 immunity in cases of covid-19 and sars, and uninfected controls. *Nature*, 584(7821):457–462, 2020.
- 21 **15.** Thomas M Snyder, Rachel M Gittelman, Mark Klinger, Damon H May, Edward J Osborne, Ruth
22 Taniguchi, H Jabran Zahid, Ian M Kaplan, Jennifer N Dines, Matthew N Noakes, et al. Magnitude
23 and dynamics of the t-cell response to sars-cov-2 infection at both individual and population levels.
24 *MedRxiv*, 2020.
- 25 **16.** Jiefei Han, Ruofei Yu, Jianchun Duan, Jin Li, Wei Zhao, Guoshuang Feng, Hua Bai, Yuqi Wang,
26 Xue Zhang, Rui Wan, et al. Weighting tumor-specific tcr repertoires as a classifier to stratify the
27 immunotherapy delivery in non–small cell lung cancers. *Science Advances*, 7(21):eabd6971, 2021.

- 1 **17.** Daria Beshnova, Jianfeng Ye, Oreoluwa Onabolu, Benjamin Moon, Wenxin Zheng, Yang-Xin Fu,
2 James Brugarolas, Jayanthi Lea, and Bo Li. De novo prediction of cancer-associated t cell receptors
3 for noninvasive cancer detection. *Science translational medicine*, 12(557), 2020.
- 4 **18.** Ryan Emerson, Anna Sherwood, Cindy Desmarais, Sachin Malhotra, Deborah Phippard, and Harlan
5 Robins. Estimating the ratio of cd4+ to cd8+ t cells using high-throughput sequence data. *Journal of*
6 *immunological methods*, 391(1-2):14–21, 2013.
- 7 **19.** Giulio Isacchini, Aleksandra M Walczak, Thierry Mora, and Armita Nourmohammad. Deep generative
8 selection models of t and b cell receptor repertoires with sonnia. *Proceedings of the National Academy*
9 *of Sciences*, 118(14), 2021.
- 10 **20.** Jason A Carter, Jonathan B Preall, Kristina Grigaityte, Stephen J Goldfless, Eric Jeffery, Adrian W
11 Briggs, Francois Vigneault, and Gurinder S Atwal. Single t cell sequencing demonstrates the functional
12 role of $\alpha\beta$ tcr pairing in cell lineage and antigen specificity. *Frontiers in immunology*, 10:1516, 2019.
- 13 **21.** Howard R Seay, Erik Yusko, Stephanie J Rothweiler, Lin Zhang, Amanda L Posgai, Martha Campbell-
14 Thompson, Marissa Vignali, Ryan O Emerson, John S Kaddis, Dave Ko, et al. Tissue distribution and
15 clonal diversity of the t and b cell repertoire in type 1 diabetes. *JCI insight*, 1(20), 2016.
- 16 **22.** Anand Murugan, Thierry Mora, Aleksandra M Walczak, and Curtis G Callan. Statistical inference of
17 the generation probability of t-cell receptors from sequence repertoires. *Proceedings of the National*
18 *Academy of Sciences*, 109(40):16161–16166, 2012.
- 19 **23.** Quentin Marcou, Thierry Mora, and Aleksandra M Walczak. High-throughput immune repertoire
20 analysis with igor. *Nature communications*, 9(1):1–10, 2018.
- 21 **24.** Yuval Elhanati, Anand Murugan, Curtis G Callan, Thierry Mora, and Aleksandra M Walczak. Quanti-
22 fying selection in immune receptor repertoires. *Proceedings of the National Academy of Sciences*,
23 111(27):9875–9880, 2014.
- 24 **25.** Zachary Sethna, Giulio Isacchini, Thomas Dupic, Thierry Mora, Aleksandra M Walczak, and Yuval
25 Elhanati. Population variability in the generation and thymic selection of t-cell repertoires. *arXiv*
26 *preprint arXiv:2001.02843*, 2020.

- 1 **26.** Junyoung Chung, Çağlar Gülçehre, KyungHyun Cho, and Yoshua Bengio. Empirical evaluation of
2 gated recurrent neural networks on sequence modeling. *CoRR*, abs/1412.3555, 2014.
- 3 **27.** Emmi Jokinen, Jani Huuhtanen, Satu Mustjoki, Markus Heinonen, and Harri Lähdesmäki. Determinin-
4 ing epitope specificity of t cell receptors with tcrgp. *BioRxiv*, page 542332, 2019.
- 5 **28.** William D Chronister, Austin Crinklaw, Swapnil Mahajan, Randi Vita, Zeynep Koşaloğlu-Yalçın,
6 Zhen Yan, Jason A Greenbaum, Leon E Jessen, Morten Nielsen, Scott Christley, et al. Tcrmatch:
7 Predicting t-cell receptor specificity based on sequence similarity to previously characterized receptors.
8 *Frontiers in immunology*, 12:673, 2021.
- 9 **29.** Kristian Davidsen, Branden J Olson, William S DeWitt III, Jean Feng, Elias Harkins, Philip Bradley,
10 and Frederick A Matsen IV. Deep generative models for t cell receptor protein sequences. *Elife*,
11 8:e46935, 2019.
- 12 **30.** K Christopher Garcia and Erin J Adams. How the t cell receptor sees antigen—a structural view. *Cell*,
13 122(3):333–336, 2005.
- 14 **31.** Kai W Wucherpfennig, Etienne Gagnon, Melissa J Call, Eric S Huseby, and Matthew E Call. Structural
15 biology of the t-cell receptor: insights into receptor assembly, ligand recognition, and initiation of
16 signaling. *Cold Spring Harbor perspectives in biology*, 2(4):a005140, 2010.
- 17 **32.** Sepp Hochreiter and Jürgen Schmidhuber. Long short-term memory. *Neural computation*, 9(8):1735–
18 1780, 1997.
- 19 **33.** Jacob Devlin, Ming-Wei Chang, Kenton Lee, and Kristina Toutanova. Bert: Pre-training of deep
20 bidirectional transformers for language understanding. *arXiv preprint arXiv:1810.04805*, 2018.
- 21 **34.** Ashish Vaswani, Noam Shazeer, Niki Parmar, Jakob Uszkoreit, Llion Jones, Aidan N Gomez, Ł ukasz
22 Kaiser, and Illia Polosukhin. Attention is all you need. In I. Guyon, U. V. Luxburg, S. Bengio,
23 H. Wallach, R. Fergus, S. Vishwanathan, and R. Garnett, editors, *Advances in Neural Information*
24 *Processing Systems*, volume 30. Curran Associates, Inc., 2017.
- 25 **35.** James Douglas Hamilton. *Time series analysis*. Princeton university press, 2020.

- 1 **36.** Razvan Pascanu, Tomás Mikolov, and Yoshua Bengio. Understanding the exploding gradient problem.
2 *CoRR*, abs/1211.5063, 2012.
- 3 **37.** Jung-Eun Shin, Adam J Riesselman, Aaron W Kollasch, Conor McMahon, Elana Simon, Chris Sander,
4 Aashish Manglik, Andrew C Kruse, and Debora S Marks. Protein design and variant prediction using
5 autoregressive generative models. *Nature communications*, 12(1):1–11, 2021.
- 6 **38.** Tomas Mikolov, Kai Chen, Greg Corrado, and Jeffrey Dean. Efficient estimation of word representa-
7 tions in vector space. *arXiv preprint arXiv:1301.3781*, 2013.
- 8 **39.** Ryan O Emerson, William S DeWitt, Marissa Vignali, Jenna Gravley, Joyce K Hu, Edward J Osborne,
9 Cindy Desmarais, Mark Klinger, Christopher S Carlson, John A Hansen, et al. Immunosequencing
10 identifies signatures of cytomegalovirus exposure history and hla-mediated effects on the t cell
11 repertoire. *Nature genetics*, 49(5):659–665, 2017.
- 12 **40.** Yumei Xiong and Rémy Bosselut. Cd4–cd8 differentiation in the thymus: connecting circuits and
13 building memories. *Current opinion in immunology*, 24(2):139–145, 2012.
- 14 **41.** Mikhail Shugay, Dmitriy V Bagaev, Ivan V Zvyagin, Renske M Vroomans, Jeremy Chase Crawford,
15 Garry Dolton, Ekaterina A Komech, Anastasiya L Sycheva, Anna E Koneva, Evgeniy S Egorov, et al.
16 Vdjdb: a curated database of t-cell receptor sequences with known antigen specificity. *Nucleic acids*
17 *research*, 46(D1):D419–D427, 2018.
- 18 **42.** Leland McInnes, John Healy, and James Melville. Umap: Uniform manifold approximation and
19 projection for dimension reduction. *arXiv preprint arXiv:1802.03426*, 2018.
- 20 **43.** Jacob Glanville, Huang Huang, Allison Nau, Olivia Hatton, Lisa E Wagar, Florian Rubelt, Xuhuai
21 Ji, Arnold Han, Sheri M Krams, Christina Pettus, et al. Identifying specificity groups in the t cell
22 receptor repertoire. *Nature*, 547(7661):94–98, 2017.
- 23 **44.** Mikhail V Pogorelyy and Mikhail Shugay. A framework for annotation of antigen specificities in
24 high-throughput t-cell repertoire sequencing studies. *Frontiers in immunology*, 10:2159, 2019.
- 25 **45.** Paul-Gydeon Ritvo, Ahmed Saadawi, Pierre Barennes, Valentin Quiniou, Wahiba Chaaara, Karim
26 El Soufi, Benjamin Bonnet, Adrien Six, Mikhail Shugay, Encarnita Mariotti-Ferrandiz, et al. High-

- 1 resolution repertoire analysis reveals a major bystander activation of tfh and tfr cells. *Proceedings of*
2 *the National Academy of Sciences*, 115(38):9604–9609, 2018.
- 3 **46.** Dmitry V Bagaev, Renske MA Vroomans, Jerome Samir, Ulrik Stervbo, Cristina Rius, Garry Dolton,
4 Alexander Greenshields-Watson, Meriem Attaf, Evgeny S Egorov, Ivan V Zvyagin, et al. Vdjdb
5 in 2019: database extension, new analysis infrastructure and a t-cell receptor motif compendium.
6 *Nucleic Acids Research*, 48(D1):D1057–D1062, 2020.
- 7 **47.** Janine Kah, Sarene Koh, Tassilo Volz, Erica Ceccarello, Lena Allweiss, Marc Lütgehetmann, Antonio
8 Bertoletti, Maura Dandri, et al. Lymphocytes transiently expressing virus-specific t cell receptors
9 reduce hepatitis b virus infection. *The Journal of clinical investigation*, 127(8):3177–3188, 2017.
- 10 **48.** Anangi Balasiddaiah, Haleh Davanian, Soo Aleman, Anna Pasetto, Lars Frelin, Matti Sällberg, Volker
11 Lohmann, Sarene Koh, Antonio Bertoletti, and Margaret Chen. Hepatitis c virus-specific t cell receptor
12 mrna-engineered human t cells: impact of antigen specificity on functional properties. *Journal of*
13 *virology*, 91(9):e00010–17, 2017.
- 14 **49.** Steven A Rosenberg, Nicholas P Restifo, James C Yang, Richard A Morgan, and Mark E Dudley.
15 Adoptive cell transfer: a clinical path to effective cancer immunotherapy. *Nature Reviews Cancer*,
16 8(4):299–308, 2008.
- 17 **50.** Steven A Rosenberg and Nicholas P Restifo. Adoptive cell transfer as personalized immunotherapy
18 for human cancer. *Science*, 348(6230):62–68, 2015.
- 19 **51.** James L Riley, Carl H June, and Bruce R Blazar. Human t regulatory cell therapy: take a billion or so
20 and call me in the morning. *Immunity*, 30(5):656–665, 2009.
- 21 **52.** Connor Shorten and Taghi M Khoshgoftaar. A survey on image data augmentation for deep learning.
22 *Journal of Big Data*, 6(1):1–48, 2019.
- 23 **53.** Edward Ma. Nlp augmentation. <https://github.com/makcedward/nlpaug>, 2019.
- 24 **54.** John-William Sidhom, H Benjamin Larman, Drew M Pardoll, and Alexander S Baras. Deeptcr
25 is a deep learning framework for revealing sequence concepts within t-cell repertoires. *Nature*
26 *communications*, 12(1):1–12, 2021.

- 1 **55.** Sofie Gielis, Pieter Moris, Wout Bittremieux, Nicolas De Neuter, Benson Ogunjimi, Kris Laukens,
2 and Pieter Meysman. Detection of enriched t cell epitope specificity in full t cell receptor sequence
3 repertoires. *Frontiers in immunology*, 10:2820, 2019.
- 4 **56.** Hsueh-Ling Janice Oh, Adeline Chia, Cynthia Xin Lei Chang, Hoe Nam Leong, Khoon Lin Ling,
5 Gijsbert M Grotenbreg, Adam J Gehring, Yee Joo Tan, and Antonio Bertoletti. Engineering t cells
6 specific for a dominant severe acute respiratory syndrome coronavirus cd8 t cell epitope. *Journal of*
7 *virology*, 85(20):10464–10471, 2011.
- 8 **57.** Pieter Moris, Joey De Pauw, Anna Postovskaya, Sofie Gielis, Nicolas De Neuter, Wout Bittremieux,
9 Benson Ogunjimi, Kris Laukens, and Pieter Meysman. Current challenges for unseen-epitope
10 tcr interaction prediction and a new perspective derived from image classification. *Briefings in*
11 *Bioinformatics*, 22(4):bbaa318, 2021.
- 12 **58.** Diederik P Kingma and Jimmy Ba. Adam: A method for stochastic optimization. *arXiv preprint*
13 *arXiv:1412.6980*, 2014.
- 14 **59.** Adam Paszke, Sam Gross, Soumith Chintala, Gregory Chanan, Edward Yang, Zachary DeVito,
15 Zeming Lin, Alban Desmaison, Luca Antiga, and Adam Lerer. Automatic differentiation in pytorch.
16 2017.